

Article

Analysis of the Anti-Corrosion Performance of Dextrin and Its Graft Copolymer on J55 Steel in Acid Solution

Mingxing Liu *, Dayu Xia, Ambrish Singh * and Yuanhua Lin

School of Materials Science and Engineering, Southwest Petroleum University, Chengdu 610500, China; xdy5657303@163.com (D.X.); yhlin28@163.com (Y.L.)

* Correspondence: m1763902986@163.com (M.L.); vishisingh4uall@gmail.com (A.S.)

Abstract: This paper studies the corrosion inhibition performance and mechanism of dextrin (Dxt) and its graft copolymer with caprolactam (Dxt-g-CPL) on J55 steel in 1 M HCl solution. Caprolactam is grafted and copolymerized with dextrin by a chemical synthesis method, to obtain a dextrin graft copolymer corrosion inhibitor. The composition of the synthesized graft copolymer was characterized by FTIR to identify whether the grafting was successful. Through weightlessness, electrochemical impedance spectroscopy (EIS), potentiodynamic polarization curve (TAFEL), scanning electrochemical microscope (SECM), scanning electron microscope (SEM), and contact angle experiments, the graft copolymer to J55 steel in 1 M HCl solution and the corrosion inhibition performance were evaluated. Moreover, we discuss its corrosion inhibition mechanism. The dextrin graft copolymer has good corrosion inhibition performance for J55 in 1 M HCl solution. When the concentration of the corrosion inhibitor increases, the corrosion inhibition efficiency will also increase. At a certain concentration, when the temperature rises, the corrosion inhibition efficiency will gradually decrease. When the concentration is 300 mg/L, it has a better corrosion inhibition effect, and the corrosion inhibition efficiency is 82.38%. Potential polarization studies have shown that Dxt-g-CPL is a mixed corrosion inhibitor, which inhibits both the cathode and the anode of the electrode reaction. SEM, SECM, and contact angle analysis results show that Dxt-g-CPL can significantly inhibit corrosion. Compared with Dxt, Dxt-g-CPL has a better inhibitory effect.

Keywords: dextrin; graft copolymer; caprolactam; inhibitor; adsorption mechanism



Citation: Liu, M.; Xia, D.; Singh, A.; Lin, Y. Analysis of the Anti-Corrosion Performance of Dextrin and Its Graft Copolymer on J55 Steel in Acid Solution. *Processes* **2021**, *9*, 1642. <https://doi.org/10.3390/pr9091642>

Academic Editor: Géraldine Gouhier

Received: 17 July 2021

Accepted: 31 August 2021

Published: 13 September 2021

Publisher's Note: MDPI stays neutral with regard to jurisdictional claims in published maps and institutional affiliations.



Copyright: © 2021 by the authors. Licensee MDPI, Basel, Switzerland. This article is an open access article distributed under the terms and conditions of the Creative Commons Attribution (CC BY) license (<https://creativecommons.org/licenses/by/4.0/>).

1. Introduction

J55 steel is a kind of carbon steel. It is low cost, has very good performance, and is widely used in various fields of life, including in petrochemical and marine development [1,2]. However, carbon steel easily reacts with various corrosive media in the environment and is destroyed, especially in the industrial process of oil-well acidification, pickling, and acid descaling. When the metal comes into contact with the acid medium, it will chemically/electrochemically react with the acid medium, causing the metal to be destroyed [3]. Therefore, the carbon steel corrosion in acidic medium is an important task of scientific research [4]. Isolating the metal from the corrosive medium is the most effective protection method. It can be used to control the corrosion process by adding coatings, cathode plate protection, and adding corrosion inhibitors. Among them, corrosion inhibitors are one of the most widely used methods [5–9].

Organic or inorganic corrosion inhibitors are adsorbed on the metal surface to form a thin film on the metal surface, to achieve the effect of inhibiting corrosion [10,11]. Among the various methods of inhibiting corrosion, the corrosion inhibitor has a good anti-corrosion effect, simple operation, low dosage, quick effect, and relatively low cost. It is also a very important anti-corrosion method in the oil and gas field [12,13]. However, most of the most widely used corrosion inhibitors are mainly chemical synthesis and have good corrosion inhibition effects. At present, there are still many problems, such as it is not easily

biodegradable, and it is harmful to organisms and the environment after discharge. Therefore, environmentally friendly corrosion inhibitors have become an important direction of scientific research. Many natural polymers found in plants are eco-friendly and not easy to pollute the environment. They can be used as effective corrosion inhibitors. The graft modification and modification of natural polymers has also become a research hotspot.

In recent years, many polymers have been a widespread concern, in terms of corrosion protection [14–21]. Many natural polysaccharides and their modified polymers are non-toxic, biodegradable, and have multiple adsorption sites, making their adsorption performance stronger than monomers. They can be used as corrosion inhibitors [22] and coating materials [23]. Moreover, many are natural polymers [24–30]; for example, natural secretion gum [31–33], pectin [34], cellulose derivatives [35,36], chitosan [37,38], mango gum, xanthan gum [39], and so on. However, it is still very necessary to develop more efficient and environmentally friendly corrosion inhibitors.

This paper mainly studies the corrosion inhibition effect of Dxt and Dxt-g-CPL as corrosion inhibitors on J55 steel in 1 M HCl medium. Dextrin is a polysaccharide compound, which is environmentally friendly and has a certain corrosion inhibition effect. There are many studies on grafting monomers on polysaccharides, and there are relatively complete synthetic methods for the synthesis of polymers. The grafted copolymer has more adsorption sites, so it has a stronger adsorption capacity than simple polysaccharides. The synthesized copolymer was characterized by FTIR, the corrosion inhibition performance of Dxt and Dxt-g-CPL was characterized by the weight loss method, EIS and TAFEL, and the metal surface was characterized by SECM, SEM, and contact angle. Finally, the corrosion inhibition mechanism of Dxt and Dxt-g-CPL on J55 steel in acid medium is analyzed.

2. Experiment

2.1. Preparation of Experimental Chemicals and Materials

The composition of J55 steel is as follows (wt.%): C = 0.34, Si = 0.20, Mn = 1.25, P = 0.020, S = 0.015, Cr = 0.150, Ni = 0.20, Cu = 0.020, and the balance Fe. Before the test, sandpaper of different roughness was used to sand the surface until there were no obvious scratches. Then the surface of the sample was cleaned with deionized water and absolute ethanol, and dried, and finally the sample was stored in a desiccator for later use. The corrosive medium was 1 M HCl.

2.2. Synthesis of Dextrin Graft Copolymer

One gram of dextrin, 10 g of caprolactam, and 0.005 g of potassium persulfate were weighed to dissolve in 100 mL, 15 mL, and 5 mL of deionized water. This was stirred in a 75 °C water bath for 20 min to completely dissolve the solid matter. The potassium persulfate solution was added to the dextrin solution, stirred in a water bath at 75 °C for 15 min, and finally the monomer caprolactam was slowly added. Under the condition of heating in a water bath, the reaction ended after 1 h. DCM was added to the reaction to precipitate, filter, and then the obtained copolymer was washed with absolute ethanol and deionized water, and part of the by-products was removed. It was dried in a vacuum drying oven at 60 °C for later use. Synthesis scheme and the molecular structure are shown in Figure 1 [31].

Chain growth reaction mechanism shown in Figure 2 [40].

2.3. Structural Characterization of the Copolymer

Through FTIR, the different characteristics of the spectrum were analyzed, and the characteristic functional groups of the dextrin-grafted caprolactam copolymer were detected, and then whether the caprolactam is successfully grafted on the dextrin was judged. A small amount of dextrin-grafted caprolactam copolymer powder was mixed with KBr powder and grinded evenly, and then compressed into tablets with a FW-4A 12-ton tablet press, and then tested. The wave number range 4000~400 cm⁻¹ was tested.

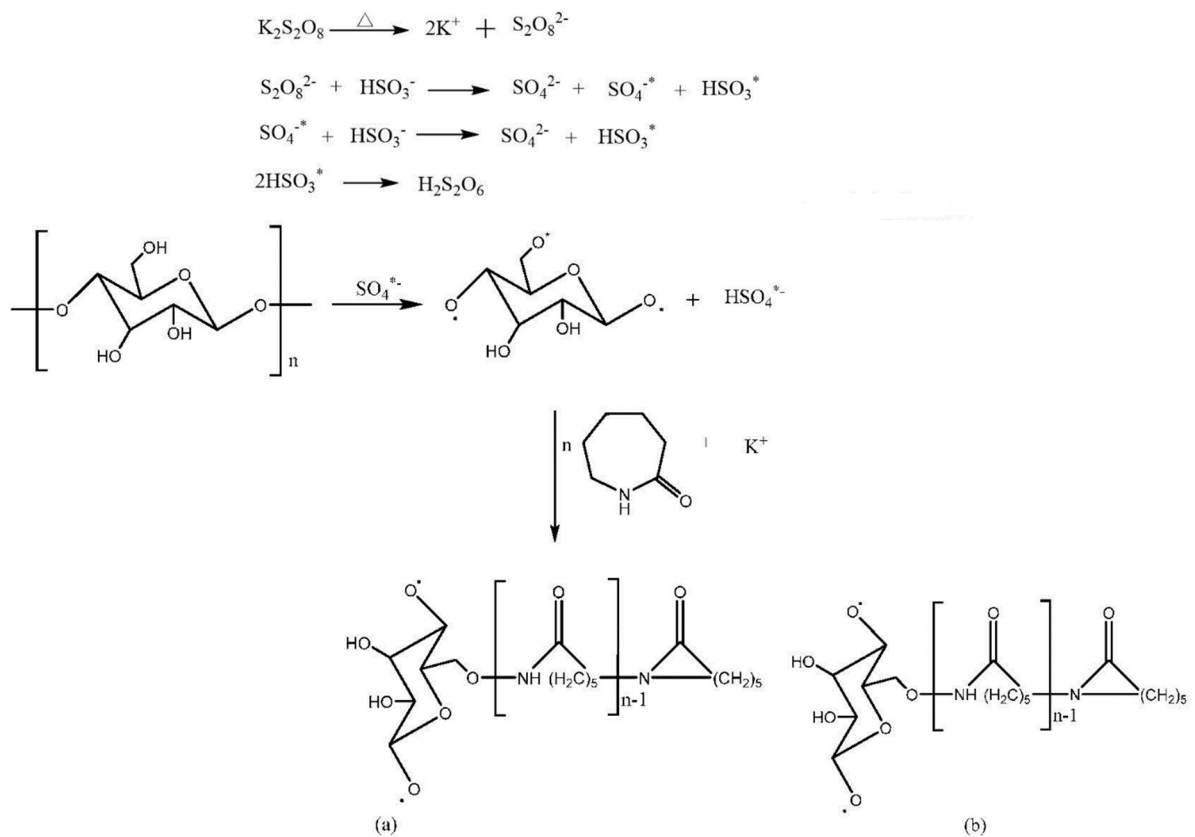


Figure 1. Synthesis scheme and polymer molecular structure diagram.

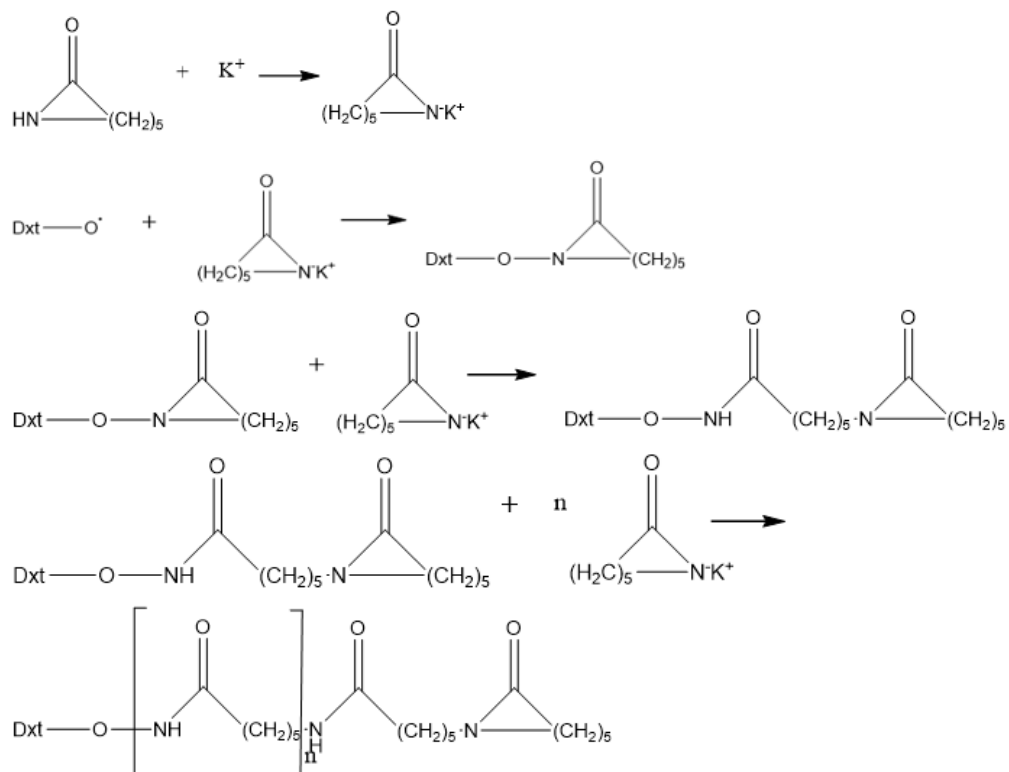


Figure 2. Chain growth reaction mechanism.

2.4. Copolymer Corrosion Inhibition Performance Test

2.4.1. Static Weightlessness Test

Before the experiment, the fully polished sample was cleaned with absolute ethanol, dried with a blower, weighed with an analytical balance (± 0.0001 g), and the original weight was recorded. During the experiment, the concentrations of Dxt and Dxt-g-CPL were 100 mg/L, 200 mg/L, 300 mg/L, 400 mg/L, the temperature was 25 °C, 35 °C, 45 °C, 55 °C, 65 °C. The experimental pressure was normal pressure (1 atm = 101.325 kPa). The corrosion time was 24 h, and three sets of samples were prepared and three sets of parallel experiments were conducted to ensure the repeatability and credibility of the experiment. After the corrosion of the sample, a film-removal solution was used to remove various corrosion products on the surface, then it was cleaned with absolute ethanol, then dried, and finally it was weighed with an analytical balance, and the experimental data were carefully recorded.

The corrosion rate C_R and the corrosion inhibition rate $\eta\%$ of the corrosion inhibitor can be calculated by the following formula [31,41]:

$$C_R = \frac{W_a - W_b}{S \Delta t} \quad (1)$$

where C_R is the corrosion rate, the unit is $\text{mg}/(\text{cm}^2 \text{ h})$; W_a and W_b are the weight of the sample before and after corrosion, respectively, the unit is mg; S is the area exposed to the solution in cm^2 ; Δt is the corrosion time, the unit is h.

$$\eta\% = \frac{C_R^0 - C_R^{inh}}{C_R^0} \times 100\%$$

where η is the corrosion inhibition efficiency after adding the corrosion inhibitor, and C_R^0 and C_R^{inh} are the corrosion rates when no corrosion inhibitor is added and when the corrosion inhibitor is added, respectively.

2.4.2. Electrochemical Test

Electrochemical analysis was carried out using a three-electrode system. The size of the sample was 1 cm \times 1 cm \times 1 cm. One side of the steel sample was welded to a copper wire, and the sample was sealed with epoxy resin and a test area of 1 cm^2 was reserved. EIS experimental sweep frequency range of 100 kHz~10 MHz and perturbation signal amplitude 10 mV were used. The Tafel polarization curve also uses a three-electrode system. The EIS results were fitted by ZsimDemo software, and the data were graphed and processed by Origin software.

Inhibition efficiency calculated by the following formula:

$$\eta\% = \frac{R_{ct}^{inh} - R_{ct}^0}{R_{ct}^{inh}} \times 100\%$$

$$\eta\% = \frac{i_{corr}^0 - i_{corr}^{inh}}{i_{corr}^0} \times 100\%$$

where R_{ct}^{inh} and R_{ct}^0 are the charge transfer resistance with and without corrosion inhibitor, Ω/cm^2 , respectively; i_{corr}^{inh} and i_{corr}^0 are the corrosion current density with and without corrosion inhibitor, A/cm^2 , respectively.

2.4.3. Scanning Electrochemical Microscope

The J55 steel sample was soaked in 1 M HCl blank solution and 300 mg/L Dxt and Dxt-g-CPL corrosion inhibitor solution for 12 h, and then subjected to SECM test to analyze the surface current. The sample size used in the experiment was 10 mm \times 10 mm \times 10 mm, a four-electrode system was adopted, the probe current was in feedback mode, probe

potential was set to 0.5 V, sensitivity to 1.0×10^{-6} A/V, and the scanning area was $200 \times 200 \mu\text{m}$. The test was carried out at 25°C and 101.325 kPa.

2.4.4. Scanning Electron Microscope–Energy Spectrum Test

Before the test, the J55 steel sample was soaked in 1 M HCl solution with and without corrosion inhibitor for 24 h. The scanning electrochemical microscope was used to observe the surface morphology under vacuum conditions, and the magnification was 1.00 KX.

2.4.5. Contact Angle Test

The J55 sample was polished step by step with sandpaper until it was smooth without obvious scratches, and then soaked in a 1 M HCl solution containing no corrosion inhibitor and containing 300 mg/L Dxt and Dxt-g-CPL corrosion inhibitors. After taking out the sample, the contact angle of pure water on the corroded J55 steel surface was measured. The test was carried out at 25°C and 101.325 kPa.

3. Results and Discussion

3.1. Characterization of Dextrin Grafted Caprolactam Copolymer

Figure 3 is the FTIR test chart of dextrin and dextrin-grafted caprolactam copolymer. In the Dxt spectrum, at 3392 cm^{-1} is the O–H stretching peak of the alcoholic hydroxyl group on the Dxt molecular chain, 2923 cm^{-1} and 2850 cm^{-1} are the C–H vibration peaks, 1080 cm^{-1} is the C–O–C stretching vibration peak, and the position at 650 cm^{-1} is the flexural vibration peak of O–H. In the spectrum of Dxt-g-CPL, the stretching vibration peak of the N–H bond and the C–H stretching vibration peak in the amide are covered in the broad peak at 3392 cm^{-1} , the C–N stretching vibration peak at 1450 cm^{-1} , the C=O stretching vibration peak at 1639 cm^{-1} , and other characteristic peaks at 986 cm^{-1} , such as the C–H out-of-plane bending vibration. The existence of these characteristic peaks in the spectrum of Dxt-g-CPL proves that caprolactam is successfully grafted onto the dextrin matrix.

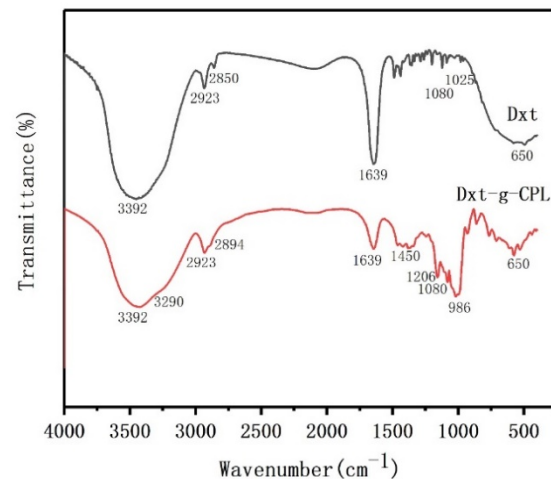


Figure 3. FTIR diagram of Dxt and Dxt-g-CPL.

3.2. Weightlessness Experiment

3.2.1. The effect of Concentration

Figure 4 shows the corrosion rate and inhibition efficiency of J55 steel added with different concentrations of Dxt and Dxt-g-CPL in 1 M HCl solution. It can be observed from the figure that at room temperature, when the concentration of the added corrosion inhibitor increases, the corrosion rate will decrease and the corrosion inhibition efficiency will increase. When the concentration of the added corrosion inhibitor reaches 300 mg/L, the corrosion inhibition efficiency of Dxt and Dxt-g-CPL reaches the highest at this time, 67.30%

and 83.27%, respectively. This shows that Dxt and Dxt-g-CPL have corrosion inhibition effects on J55 steel. Comparing the two, Dxt-g-CPL has better corrosion inhibition effects.

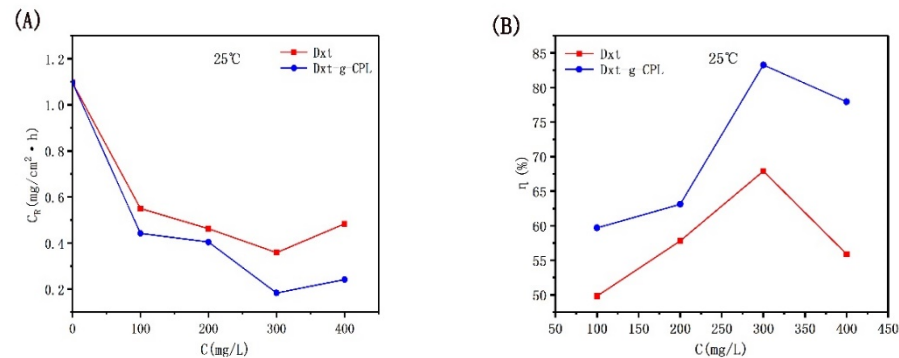


Figure 4. CR and η of J55 steel added with different concentrations of corrosion inhibitor in 1 M HCl solution. (A) Dxt; (B) Dxt-g-CPL.

3.2.2. The Influence of Temperature

Figure 5 shows the corrosion rate and corrosion inhibition efficiency of J55 steel with temperature changes when no corrosion inhibitor is added and when 300 mg/L Dxt and Dxt-g-CPL are added to the 1 M HCl solution. It can be observed from the figure that under the same corrosion inhibitor concentration, as the temperature continues to increase, the corrosion rate gradually increases, and the corrosion inhibition efficiency gradually decreases. When the temperature rises, due to the intensification of molecular motion, the corrosion inhibitor adsorption protective film that formed on the metal surface will be desorbed, resulting in a decrease in coverage and a reduction in corrosion inhibition efficiency.

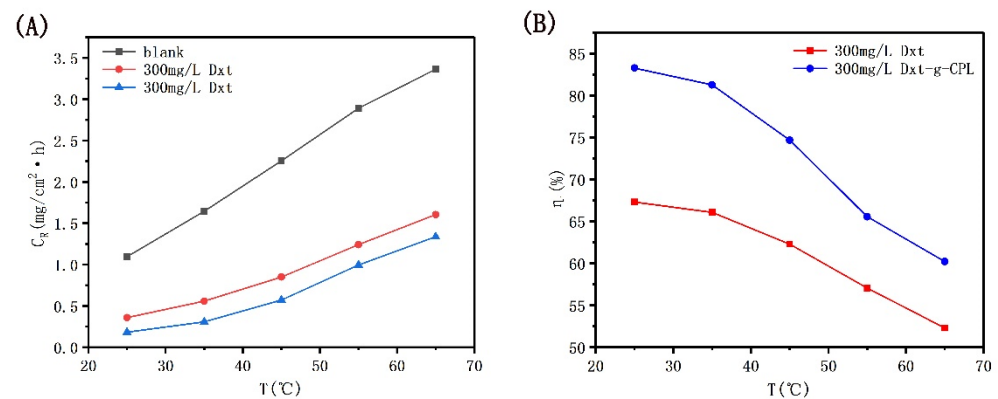


Figure 5. CR and η of J55 steel in 1 M HCl solution with different corrosion inhibitors as a function of temperature. (A) T-CR; (B) T- η .

3.3. Electrochemical Studies

3.3.1. Open circuit Potential Analysis

Figure 6 shows the open circuit potential of J55 steel added with 300 mg/L of Dxt and Dxt-g-CPL, and immersed in a 1 M HCl solution for 30 min. The initial open circuit potential fluctuates, and the amplitude of the fluctuation is relatively large. As the standing time increases, the potential gradually stabilizes, indicating that the solution system has reached a stable state. After adding the corrosion inhibitor, the open circuit potentials all shifted to the positive direction. This shows that a layer of corrosion inhibitor molecules is adsorbed on the surface of J55 steel, to form a protective film, thereby protecting the metal from corrosion by corrosive media, thereby inhibiting the reaction of the cathode.

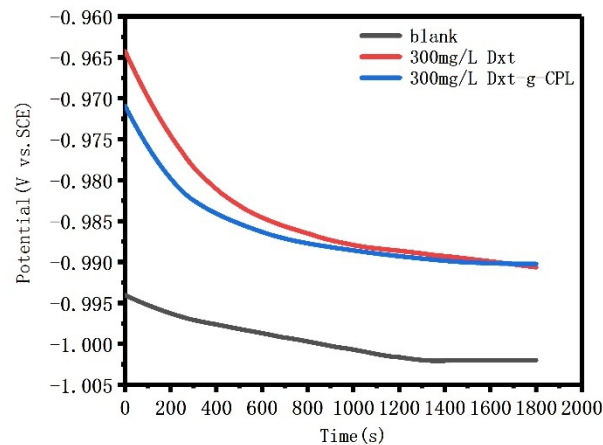


Figure 6. The open circuit potential of J55 steel with Dex and Dex-g-CPL added to 1 M HCl solution.

3.3.2. Electrochemical Impedance Spectroscopy

Figure 7 shows Nyquist and Bode diagrams of J55 steel in 1 M HCl solution, with different concentrations of Dxt and Dxt-g-CPL. As shown in the figure, after adding different concentrations of Dxt and Dxt-g-CPL to 1 M HCl solution, the impedance of J55 steel changes greatly. Comparing Nyquist with different concentrations of corrosion inhibitors and the blank group, there are semi-circular arcs and both appear flat. When more and more corrosion inhibitors are added, the radius of the Nyquist diagram continues to increase, but the shape of the semi-circular arc does not change significantly, indicating that the addition of Dxt and Dxt-g-CPL will affect the corrosion rate, but not change the process of the electrode reaction. The corrosion process of J55 steel is mainly controlled by charge transfer. Corrosion inhibitor molecules will be adsorbed onto the metal surface by physical or chemical behavior, hindering the charge transfer between the metal surface and the solution, and increasing the resistance during the electrode reaction process. It can be observed from the Bode diagram that after adding different concentrations of corrosion inhibitor, the absolute values of impedance and constant phase angle are both significantly larger than the blank sample, indicating that both Dxt and Dxt-g-CPL can inhibit metal corrosion.

Table 1 shows the electrochemical parameters of solution resistance R_s , charge transfer resistance R_{ct} , and constant phase angle element Q , obtained by fitting the Nyquist diagrams of Dxt and Dxt-g-CPL. The data in the table show that the values of R_{ct} , η , θ , and n all change correspondingly with the increase in the concentration. It is proved that Dxt and Dxt-g-CPL will adsorb onto the metal surface to form a protective film, thereby inhibiting the corrosion of J55 steel by corrosive media. When the concentration of Dxt and Dxt-g-CPL increases, more Dxt and Dxt-g-CPL molecules are adsorbed onto the metal surface, and the surface coverage increases. When the concentration of Dxt and Dxt-g-CPL is 300 mg/L, the corrosion inhibition efficiency reaches the maximum. Compared with Dxt, Dxt-g-CPL has a better adsorption capacity on the surface of J55 steel, more effective molecules adsorbed on the surface, and better corrosion resistance.

3.3.3. Potentiodynamic Polarization Measurements

Figure 8 shows the potentiodynamic polarization curve of J55 steel in 1 M HCl solution, with different concentrations of Dxt and Dxt-g-CPL. The figure shows that, comparing the polarization curves after adding different concentrations of corrosion inhibitors, the cathode and anode parts all move downward, but the shape of the curve hardly changes. This shows that the addition of the corrosion inhibitor inhibits the reaction of the anode and cathode at the same time, but does not change the mechanism of the electrode reaction.

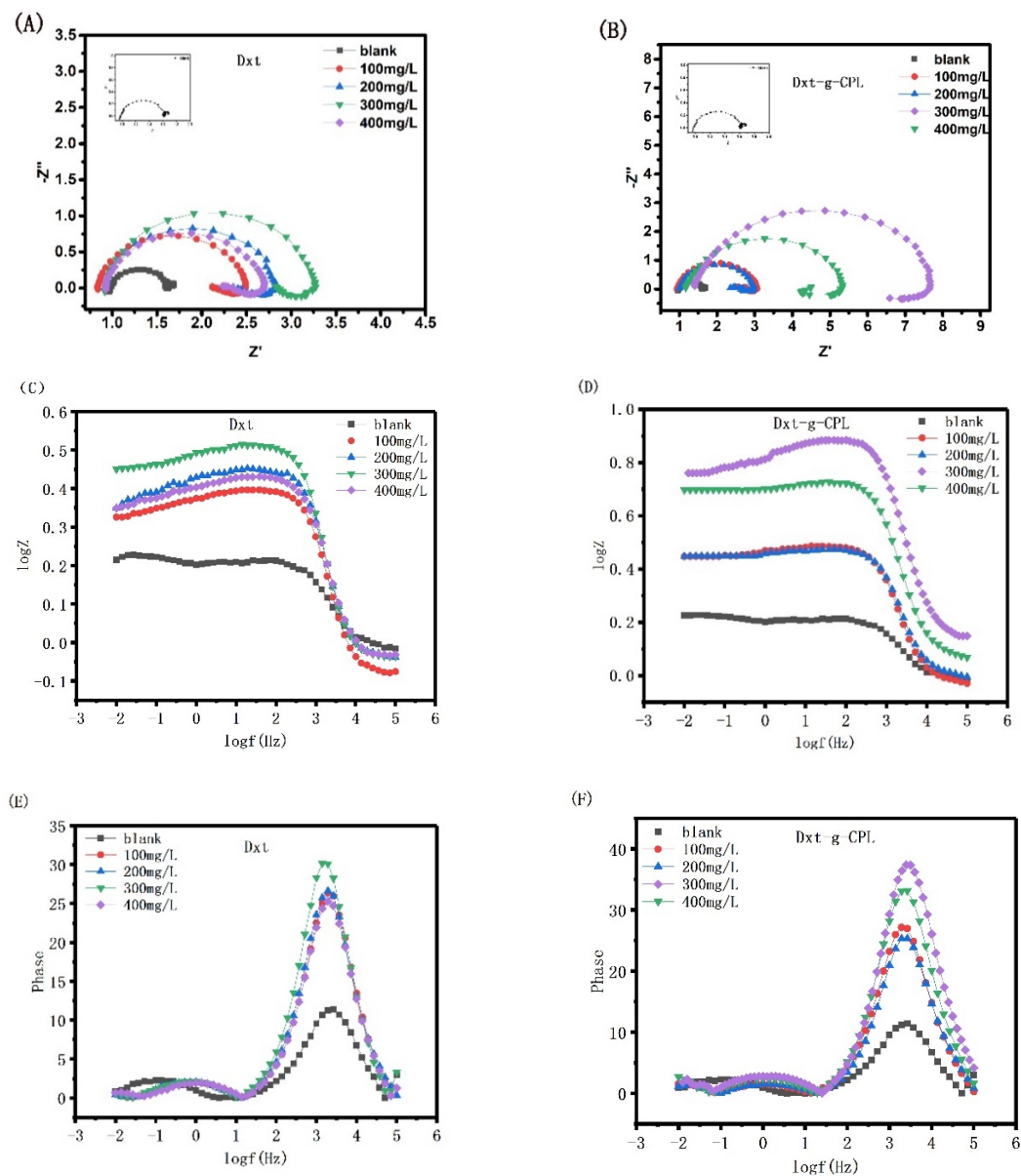


Figure 7. Nyquist and Bode diagrams of J55 steel in 1 M HCl solution with different concentrations of (A,C,E) Dxt; (B, D,F) Dxt-g-CPL.

Table 1. Nyquist diagram-related parameters of J55 steel in 1 M HCl solution with different concentrations of Dxt and Dxt-g-CPL.

Concentration (mg/L)	R_s (Ωcm^2)	CPE			R_{ct} (Ωcm^2)	R_L (Ωcm^2)	L (H cm^2)	η_R (%)
		Q ($\text{m}\Omega^{-1} \text{S}^n \text{cm}^{-2}$)	n					
blank	0.9811	0.6729	0.8527	0.6583	0.1635	0.00001168	-	
Dxt 100 mg/L	0.8383	0.1644	0.9248	1.364	0.2732	0.06177	51.71	
Dxt 200 mg/L	0.9205	0.1583	0.9237	1.502	0.3696	0.1143	56.17	
Dxt 300 mg/L	0.9227	0.1428	0.935	1.965	0.3519	0.07441	66.49	
Dxt 400 mg/L	0.9245	0.171	0.915	1.432	0.3141	0.05934	54.03	
Dxt-g-CPL 100 mg/L	0.9484	0.1644	0.8994	1.606	0.2852	0.05247	59.01	
Dxt-g-CPL 200 mg/L	1.004	0.1423	0.9073	1.811	0.3471	0.08547	63.65	
Dxt-g-CPL 300 mg/L	1.41	0.0463	0.9148	3.736	2.267	0.5813	82.38	
Dxt-g-CPL 400 mg/L	1.191	0.09234	0.8977	3.023	1.057	0.2105	78.22	

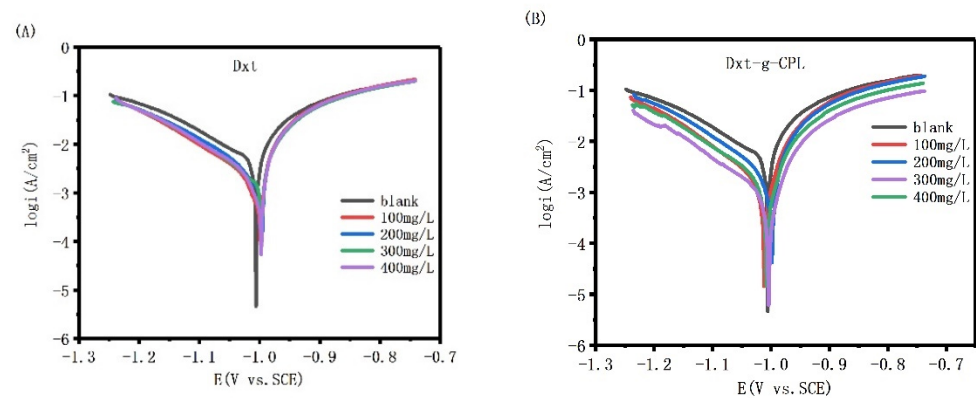


Figure 8. Potential polarization curves of J55 steel in 1 M HCl solution with different concentrations (A) Dxt; (B) Dxt-g-CPL.

The Tafel linear extrapolation method is used to fit the potentiodynamic polarization curve, and the relevant data, shown in Table 2, can be obtained. The data in the table show that the corrosion potential changes after adding Dxt and Dxt-g-CPL. Generally, the corrosion potential after adding the corrosion inhibitor and the blank corrosion potential ($\Delta E_{\text{corr}} = E_{\text{corr}} - E_{0\text{corr}}$) changes more than 85 mV, which can be regarded as a cathode or anode corrosion inhibitor. The data in the table show that if the change in the corrosion potential is less than 85 mV, Dxt and Dxt-g-CPL can be regarded as mixed corrosion inhibitors. When Dxt and Dxt-g-CPL are 300 mg/L, the corrosion current is reduced, and the corrosion inhibition efficiency also reaches 67.81% and 81.33%, respectively.

Table 2. Polarization curve-related parameters of J55 steel in 1 M HCl solution with different concentrations of Dxt and Dxt-g-CPL.

Concentration(mg/L)	b_a	b_c	$E_{\text{corr}}(\text{V/SCE})$	$I_{\text{corr}}(\text{A/cm}^2)$	η_R (%)	Surface Coverage(θ)	
blank	0.1279	0.2638	−1.010	0.0105			
Dxt	100 mg/L	0.1224	−0.997	0.00498	52.57	0.5257	
	200 mg/L	0.1134	−0.997	0.00475	54.76	0.5476	
	300 mg/L	0.0903	−0.997	0.00338	67.81	0.6781	
	400 mg/L	0.1336	0.2022	−0.998	0.00425	59.52	0.5952
	100 mg/L	0.1239	0.1996	−0.999	0.0045	57.14	0.5714
Dxt-g-CPL	200 mg/L	0.1035	−0.999	0.00383	63.52	0.6352	
	300 mg/L	0.1392	−1.000	0.00196	81.33	0.8133	
	400 mg/L	0.0978	0.1661	−1.010	0.00233	77.81	0.7781

3.4. Scanning Electrochemical Microscope

Figure 9 shows the scanning electrochemical results of J55 steel added with 300 mg/L Dxt and 300 mg/L Dxt-g-CPL into 1 M HCl solution after corrosion. Figure 9a shows that the current on the surface of the steel sample without the corrosion inhibitor has a large change, and the surface of the sample is relatively rough. Figure 9b,c show that after adding the corrosion inhibitor, the surface current has obviously decreased, indicating that the metal surface is relatively smooth. Compared with no corrosion inhibitor, there is a smaller current when the corrosion inhibitor is added. This shows that after the corrosion inhibitor is added, the corrosion inhibitor is adsorbed onto the metal surface, reducing the contact between the corrosive medium and the metal surface, thereby effectively protecting the metal surface.

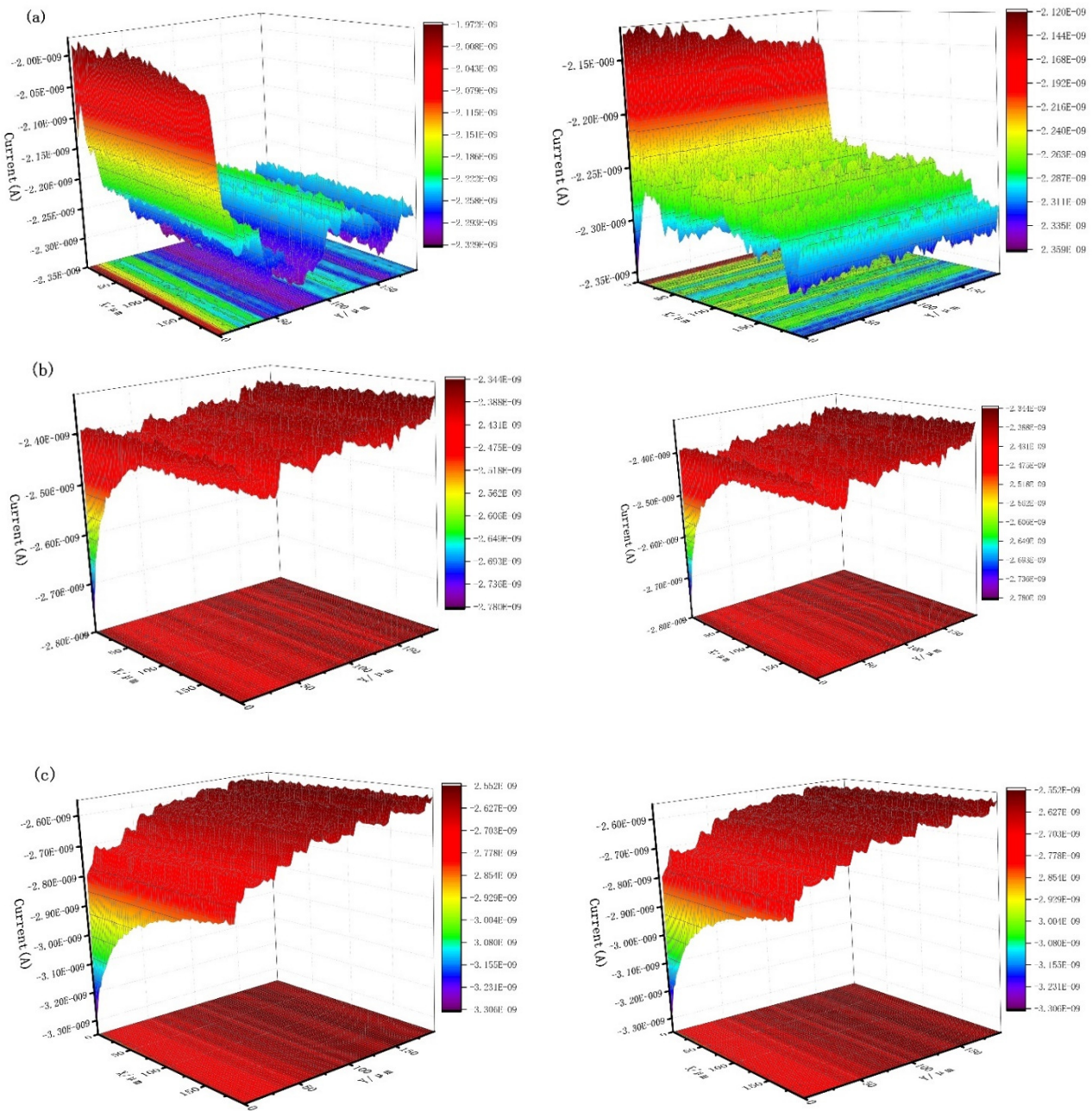


Figure 9. The x (left) direction and y (right) direction SECM of J55 steel in the 1 M HCl solution without and without adding corrosion inhibitor. (a) Blank; (b) 300 mg/L Dxt; (c) 300 mg/L Dxt-g-CPL.

3.5. Scanning Electron Microscope

Figure 10 shows the surface corrosion of J55 steel after it is immersed in different 1 M HCl solutions for 24 h. In Figure 10a, the sample is not corroded, and the surface is smooth, without impurities, only with scratches when polished. Figure 10b is a sample corroded by 1 M HCl, the surface is seriously corroded and there are many corrosion products. Figure 10c,d show the sample after adding 300 mg/L Dxt and 300 mg/L Dxt-g-CPL; the corrosion products on the surface have been significantly reduced, and it is smoother than the sample without the corrosion inhibitor. The scratches left when the surface is polished can be observed, indicating that the corrosion is suppressed. By comparing the pictures of adding different corrosion inhibitors, it is found that Dxt-g-CPL has a better corrosion inhibition effect.

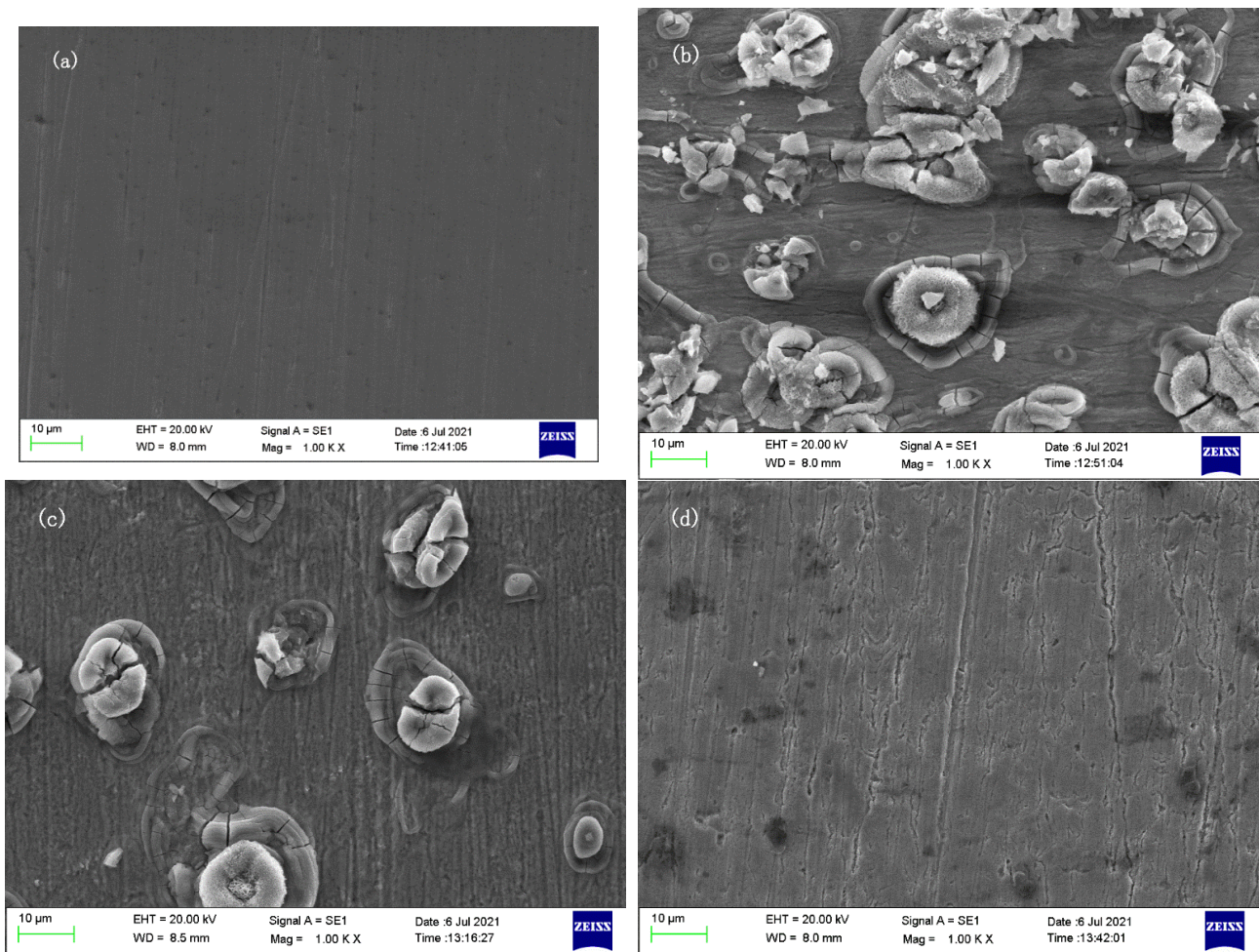


Figure 10. Surface morphology of J55 steel under different conditions. (a) Not corroded; (b) 1 M HCl; (c) 300 mg/L Dxt; (d) 300 mg/LDxt-g-CPL.

3.6. Contact Angle Measurement

Figure 11 shows the change in the contact angle of the sample surface when J55 steel is immersed in 1 M HCl solution, and 1 M HCl solution containing 300 mg/L Dxt and 300 mg/L Dxt-g-CPL, respectively. The figure shows that the contact angle of the surface after corrosion of the sample without the corrosion inhibitor is 23.4° , showing good hydrophilicity. With the addition of the corrosion inhibitor, the contact angle of the sample surface increases. After adding 300 mg/L Dxt and 300 mg/L Dxt-g-CPL, the contact angles are 71.0° and 98.4° , respectively. This is because the hydrophilic group of the corrosion inhibitor adsorbs onto the surface of the sample, to form an adsorption film, while the hydrophobic group forms a hydrophobic interface, which changes the hydrophilicity of the sample surface. This prevents the contact of the corrosive medium with the surface of the sample, and inhibits the corrosion process. Therefore, Dxt-g-CPL has a better anti-corrosion effect.



Figure 11. (a) Blank; (b) 300 mg/LDxt; (c) 300 mg/L Dxt-g-CPL.

4. Analysis of Adsorption Mechanism

4.1. Adsorption Isotherm

In order to study the interaction between the dextrin-grafted caprolactam copolymer and the metal surface, the adsorption process of Dxt-g-CPL on J55 steel was analyzed by the isotherm adsorption model. The verification found that the adsorption behavior of Dxt-g-CPL on J55 steel conforms to the Langmuir isotherm adsorption model. The following is the Langmuir adsorption isotherm equation and the calculation equation of surface coverage:

$$\frac{C}{\theta} = \frac{1}{K_{ads}} + C$$

$$\theta = \frac{\eta\%}{100}$$

where C is the concentration of corrosion inhibitor; θ is the surface coverage; and K_{ads} is the adsorption–desorption equilibrium constant.

The relationship between the standard adsorption Gibbs free energy (ΔG_{ads}^{θ}) and the adsorption–desorption equilibrium constant (K_{ads}) is shown as follows [42]:

$$\Delta G_{ads}^{\theta} = -RT \ln(1 \times 10^6 K_{ads})$$

where ΔG_{ads}^{θ} is the free energy of adsorption, kJ/mol; T is the temperature, K; and R is the molar gas constant.

$\Delta G_{ads}^{\theta} < 0$ indicates that the adsorption of Dxt-g-CPL molecules on the metal surface is a spontaneous occurrence; $|\Delta G_{ads}^{\theta}| < 20$ kJ/mol, the adsorption type can be identified as physical adsorption; $|\Delta G_{ads}^{\theta}| > 40$ kJ/mol, the adsorption type is chemical adsorption; and 20 kJ/mol $< |\Delta G_{ads}^{\theta}| < 40$ kJ/mol, the corrosion inhibitor has both physical adsorption and chemical adsorption on the metal surface [43–46].

The corrosion inhibition efficiency that was obtained by verifying the electrochemical impedance spectroscopy and TAFEL polarization curve of Dxt-g-CPL respectively conforms to the Langmuir isotherm adsorption equation. The relationship between C and C/θ is shown in Figure 12, and the adsorption parameters are shown in Table 3.

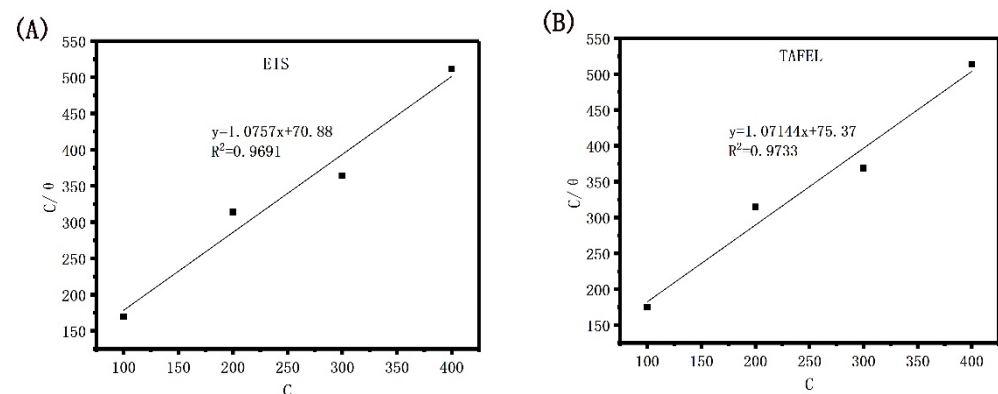


Figure 12. Langmuir isotherm adsorption model of J55 steel in 1 M HCl solution with different concentrations of Dxt-g-CPL. (A) EIS; (B) TAFEL.

Table 3. Fitting parameters obtained from Langmuir isotherm equation.

	Slope	R ²	Intercept	K _{ads}	ΔGkJ/mol
EIS	1.0757	0.9691	70.88	0.01411	−23.68
TAFEL	1.0714	0.9733	75.37	0.01327	−23.53

It can be observed from the table that the R2 values are 0.9691 and 0.9733, respectively, which are very close to one, indicating that the adsorption behavior of Dxt-g-CPL on J55 steel, at room temperature, conforms to the Langmuir isotherm adsorption model. When the free energy of adsorption is negative, the adsorption reaction of Dxt-g-CPL on the surface of J55 steel is a spontaneous process [47,48]. The free energy of the adsorption of Dxt-g-CPL is -23.68 kJ/mol and -23.53 kJ/mol, which indicates that Dxt-g-CPL has both physical adsorption and chemical adsorption on the surface of J55 steel.

4.2. Analysis of Corrosion Inhibition Mechanism

The adsorption mechanism of corrosion inhibitor molecules is recognized by most people. There are many organic functional groups in Dxt and Dxt-g-CPL molecules, and the properties of the metal surface and the d empty orbitals of the metal have a great influence on the adsorption behavior.

In the 1 M HCl solution, there is a large amount of Cl^- , and when it comes into contact with the metal surface, specific adsorption occurs. At this time, the metal surface has some negative charges, and the positively charged particles in the solution are more likely to form a protective film. The Dxt and Dxt-g-CPL molecules contain many N and O atoms, which are easy to protonate in acidic media. Therefore, corrosion inhibitors may exist in the following two forms under acidic conditions: Dxt and DxtH^{x+} , and Dxt-g-CPL and Dxt-g-CPLH^{x+} . The adsorption methods of the corrosion inhibitor molecules on the metal surface in this study may be the following:

- (1) The electrostatic interaction between the corrosion inhibitor molecules and the metal surface makes the corrosion inhibitor molecules physically adsorb onto the metal surface;
- (2) The d orbitals in the atoms on the metal surface, and the electrons of the O and N atoms in the corrosion inhibitor molecules easily form coordination bonds, so that the corrosion inhibitor molecules are chemically adsorbed onto the metal surface;
- (3) The corrosion inhibitor molecule contains functional groups, such as hydroxyl and carbonyl, which can form coordination bonds with the metal surface.

In this study, both Dxt and Dxt-g-CPL can adsorb onto the surface of J55 steel, to form an adsorption film to protect the metal surface. The Dxt-g-CPL molecule contains caprolactam molecules, which makes Dxt-g-CPL easier to be protonated, and makes it easier to form a protective film. The experimental results show that the corrosion inhibition effect of Dxt-g-CPL is better than that of Dxt, and the electron contribution ability of Dxt-g-CPL to the metal surface is greater than that of Dxt. It is proved that the grafting of caprolactam improves the corrosion inhibition performance of Dxt. All the experimental results of this study have confirmed this point.

5. Conclusions

Taking dextrin-grafted caprolactam copolymer (Dxt-g-CPL) as the research object, using the weight loss method, electrochemical research, surface morphology analysis, and isotherm adsorption model analysis, the corrosion inhibition performance of Dxt-g-CPL in 1 M HCl solution was studied. Conclusions can be drawn from the experimental and theoretical results.

(1) In 1 M HCl solution, compared with Dxt, Dxt-g-CPL has a better corrosion inhibition performance for J55 steel, and the corrosion inhibition efficiency increases with the increase in the concentration. When the concentration of Dxt-g-CPL is 300 mg/L, the corrosion inhibition efficiency is the highest, but it will decrease with the increase in the temperature.

(2) The adsorption of Dxt-g-CPL onto the surface of J55 steel follows the Langmuir adsorption isotherm model. Additionally, its adsorption mechanism is the simultaneous existence of physical adsorption and chemical adsorption.

(3) According to the analysis of the potentiodynamic polarization curve, the change in the corrosion potential is less than 85 mV, and the deviation of the corrosion potential

relative to the blank area is small, which proves that Dxt-g-CPL is a mixed corrosion inhibitor; it can suppress the electrode reaction of the cathode and anode at the same time.

(4) Scanning electron microscopy showed that compared with the metal without the corrosion inhibitor, the morphology of the metal surface with Dxt and Dxt-g-CPL was significantly improved, indicating that the synthesized graft copolymer has a better corrosion inhibition performance.

Author Contributions: Conceptualization, M.L. and A.S.; Data curation, M.L. and A.S.; Investigation, M.L. and D.X.; Project administration, A.S.; Writing—review & editing, M.L., Y.L. and D.X. All authors have read and agreed to the published version of the manuscript.

Funding: These studies are funded by the Young Science and Technology Innovation Research Group of Advanced Surface Functional Materials, Southwest Petroleum University, number -2018CXTD06.

Institutional Review Board Statement: Not applicable.

Informed Consent Statement: Not applicable.

Data Availability Statement: The data presented in this study are available on request from the corresponding author. The data are not publicly available due to privacy restriction.

Acknowledgments: The authors are thankful to the financial assistance provided by the Youth Scientific and Innovation Research Team for Advanced Surface Functional Materials, Southwest Petroleum University, number-2018CXTD06, and the research project of the State Key Laboratory of China on the safe development and efficient utilization of materials for acid oil and gas fields, Southwest Petroleum University number-G201910.

Conflicts of Interest: The authors declare no conflict of interest.

References

1. Achary, G.; Naik, Y.A.; Kumar, S.V.; Venkatesha, T.; Sherigara, B. An electroactive co-polymer as corrosion inhibitor for steel in sulphuric acid medium. *Appl. Surf. Sci.* **2008**, *254*, 5569–5573. [[CrossRef](#)]
2. De la Fuente, D.; Díaz, I.; Simancas, J.; Chico, B.; Morcillo, M. Long-term atmospheric corrosion of mild steel. *Corros. Sci.* **2011**, *53*, 604–617. [[CrossRef](#)]
3. Jeeva, M.; Prabhu, G.V.; Boobalan, M.S.; Rajesh, C.M. Interactions and Inhibition Effect of Urea-Derived Mannich Bases on a Mild Steel Surface in HCl. *J. Phys. Chem. C* **2015**, *119*, 22025–22043. [[CrossRef](#)]
4. Döner, A.; Solmaz, R.; Özcan, M.; Kardaş, G. Experimental and theoretical studies of thiazoles as corrosion inhibitors for mild steel in sulphuric acid solution. *Corros. Sci.* **2011**, *53*, 2902–2913. [[CrossRef](#)]
5. Lahiri, A.K. *Applied Metallurgy and Corrosion Control: A Handbook for the Petrochemical Industry Indian Institute of Metals Series*; Springer: Berlin/Heidelberg, Germany, 2017; p. 276.
6. Barmatov, E.; Geddes, J.; Hughes, T.; Nagl, M. Research on corrosion inhibitors for acid stimulation. In Proceedings of the CORROSION 2012, Salt Lake City, UT, USA, 11–15 March 2012.
7. Papavinasam, S. Corrosion inhibitors. In *Uhlig's Corrosion Handbook*; Revie, R.W., Ed.; Wiley: Hoboken, NJ, USA, 2011; p. 1021e32.
8. Dawson, J.L. Chemical treating in oil and gas production. In *Shreir's Corrosion*; Richardson, T., Ed.; Elsevier: Oxford, UK, 2010; p. 2900e29.
9. Abd El-Lateef, H.M.; Abbasov, V.M.; Aliyeva, L.I.; Ismayilov, T.A. Corrosion protection of steel pipelines against CO₂ corrosion—A review. *Chemother J.* **2012**, *2*, 52.
10. Balaskas, A.C.; Kartsonakis, I.A.; Snihirova, D.; Montemor, M.F.; Kordas, G. Improving the corrosion protection properties of organically modified silicate-epoxy coatings by incorporation of organic and inorganic inhibitors. *Prog. Org. Coat.* **2011**, *72*, 653. [[CrossRef](#)]
11. Yuce, A.O.; Mert, B.D.; Kardas, G.; Yazıcı, B. Electrochemical and quantum chemical studies of 2-amino-4-methyl-thiazole as corrosion inhibitor for mild steel in HCl solution. *Corros. Sci.* **2014**, *83*, 310–316. [[CrossRef](#)]
12. Helal, N.H.; Badawy, W.A. Environmentally safe corrosion inhibition of Mg–Al–Zn alloy in chloride free neutral solutions by amino acids. *Electrochim. Acta* **2011**, *56*, 6581–6587. [[CrossRef](#)]
13. Singh, A.; Soni, N.; Deyuan, Y.; Kumar, A. A combined electrochemical and theoretical analysis of environmentally benign polymer for corrosion protection of N80 steel in sweet corrosive environment. *Results Physics.* **2019**, *13*, 102–116. [[CrossRef](#)]
14. Atta, A.; El-Azabawy, O.; Ismail, H.; Hegazy, M. Novel dispersed magnetite core-shell nanogel polymers as corrosion inhibitors for carbon steel in acidic medium. *Corros. Sci.* **2011**, *53*, 1680–1689. [[CrossRef](#)]
15. Zou, C.; Yan, X.; Qin, Y.; Wang, M.; Liu, Y. Inhibiting evaluation of b-Cyclodextrin-modified acrylamide polymer on alloy steel in sulfuric solution. *Corros. Sci.* **2014**, *85*, 445–454. [[CrossRef](#)]

16. Dehghani, A.; Bahlakeh, G.; Ramezanzadeh, B. A detailed electrochemical/theoretical exploration of the aqueous Chinese gooseberry fruit shell extract as a green and cheap corrosion inhibitor for mild steel in acidic solution. *J. Mol. Liq.* **2019**, *282*, 366–384. [[CrossRef](#)]
17. Okafor, P.; Ikpi, M.; Uwah, I.; Ebenso, E.; Ekpe, U.; Umoren, S. Inhibitory action of Phyllanthus amarus extracts on the corrosion of mild steel in acidic media. *Corros. Sci.* **2008**, *50*, 2310–2317. [[CrossRef](#)]
18. Sanaei, Z.; Ramezanzadeh, M.; Bahlakeh, G.; Ramezanzadeh, B. Use of Rosa canina fruit extract as a green corrosion inhibitor for mild steel in 1 M HCl solution: A complementary experimental, molecular dynamics and quantum mechanics investigation. *J. Ind. Eng. Chem.* **2018**, *69*, 18–31. [[CrossRef](#)]
19. Dehghani, A.; Bahlakeh, G.; Ramezanzadeh, B.; Ramezanzadeh, M. Potential of Borage flower aqueous extract as an environmentally sustainable corrosion inhibitor for acid corrosion of mild steel: Electrochemical and theoretical studies. *J. Mol. Liq.* **2019**, *277*, 895–911. [[CrossRef](#)]
20. Mobin, M.; Basik, M.; Aslam, J. Pineapple stem extract (Bromelain) as an environmental friendly novel corrosion inhibitor for low carbon steel in 1 M HCl. *Measurement* **2018**, *134*, 595–605. [[CrossRef](#)]
21. Benarioua, M.; Mihi, A.; Bouzeghaia, N.; Naoun, M. Mild steel corrosion inhibition by Parsley (Petroselinum Sativum) extract in acidic media. *Egypt. J. Pet.* **2019**, *28*, 155–159. [[CrossRef](#)]
22. Zhang, H.; Wang, D.; Wang, F.; Jin, X.; Yang, T.; Cai, Z.; Zhang, J. Corrosion inhibition of mild steel in hydrochloric acid solution by quaternary ammonium salt derivatives of corn stalk polysaccharide (QAPS). *Desalination* **2015**, *372*, 57–66. [[CrossRef](#)]
23. Carneiro, J.; Tedim, J.; Ferreira, M.G.S. Chitosan as a smart coating for corrosion protection of aluminium alloy 2024: A review. *Prog. Org. Coat.* **2015**, *89*, 348–356. [[CrossRef](#)]
24. Kumar, S.; Vashisht, H.; Olasunkanmi, L.; Bahadur, I.; Verma, H.; Singh, G.; Obot, I.B.; Ebenso, E.E. Experimental and theoretical studies on inhibition of mild steel corrosion by some synthesized polyurethane tri-block co-polymers. *Sci. Rep.* **2016**, *6*, 30937. [[CrossRef](#)] [[PubMed](#)]
25. Umoren, S.A.; Eduok, U. Application of carbohydrate polymers as corrosion inhibitors for metal substrates in different media: A review. *Carbohydr. Polym.* **2016**, *140*, 314–341. [[CrossRef](#)] [[PubMed](#)]
26. Arthur, D.E.; Jonathan, A.; Ameh, P.O.; Anya, C. A review on the assessment of polymeric materials used as corrosion inhibitor of metals and alloys. *Int. J. Ind. Chem.* **2013**, *4*, 2. [[CrossRef](#)]
27. Raja, P.B.; Sethuraman, M.G. Natural products as corrosion inhibitor for metals in corrosive media—A review. *Mater. Lett.* **2008**, *62*, 113–116. [[CrossRef](#)]
28. Biswas, A.; Das, D.; Lgaz, H.; Pal, S.; Udayabhanu, U.G. Biopolymer dextrin and poly (vinyl acetate) based graft copolymer as an efficient corrosion inhibitor for mild steel in hydrochloric acid: Electrochemical, surface morphological and theoretical studies. *J. Mol. Liq.* **2018**, *275*, 867–878. [[CrossRef](#)]
29. Das, D.; Mukherjee, S.; Pal, A.; Das, R.; Sahu, S.G.; Pal, S. Synthesis and characterization of biodegradable copolymer derived from dextrin and poly(vinyl acetate) via atom transfer radical polymerization. *RSC Adv.* **2015**, *6*, 9352–9359. [[CrossRef](#)]
30. Biswas, A.; Mourya, P.; Mondal, D.; Pal, S.; Udayabhanu, G. Grafting effect of gum acacia on mild steel corrosion in acidic medium: Gravimetric and electrochemical study. *J. Mol. Liq.* **2018**, *251*, 470–479. [[CrossRef](#)]
31. Biswas, A.; Pal, S.; Udayabhanu, G. Experimental and theoretical studies of xanthan gum and its graft co-polymer as corrosion inhibitor for mild steel in 15% HCl. *Appl. Surf. Sci.* **2015**, *353*, 173–183. [[CrossRef](#)]
32. Abdallah, M. Guar Gum as Corrosion Inhibitor for Carbon Steel in Sulfuric Acid Solutions. *Port. Electrochimica Acta* **2004**, *22*, 161–175. [[CrossRef](#)]
33. Singh, A.; Mohamed, H.S.; Singh, S.; Yu, H.; Lin, Y. Corrosion inhibition using guar gum grafted 2-acrylamido-2-methylpropanesulfonic acid (GG-AMPS) in tubular steel joints. *Constr. Build. Mater.* **2020**, *258*, 119728. [[CrossRef](#)]
34. Fiori-Bimbi, M.V.; Alvarez, P.E.; Vaca, H.; Gervasi, C.A. Corrosion inhibition of mild steel in HCL solution by pectin. *Corros. Sci.* **2015**, *92*, 192–199. [[CrossRef](#)]
35. Solomon, M.; Umoren, S.; Udosoro, I.; Udoh, A. Inhibitive and adsorption behaviour of carboxymethyl cellulose on mild steel corrosion in sulphuric acid solution. *Corros. Sci.* **2010**, *52*, 1317–1325. [[CrossRef](#)]
36. Rajeswari, V.; Kesavan, D.; Gopiraman, M.; Viswanathamurthi, P. Physicochemical studies of glucose, gellan gum, and hydroxypropyl cellulose—inhibition of castiron corrosion. *Carbohydr. Polym.* **2013**, *95*, 288–294. [[CrossRef](#)] [[PubMed](#)]
37. Bahari, H.S.; Ye, F.; Carrillo, E.A.T.; Leliopoulos, C.; Savaloni, H.; Dutta, J. Chitosan nanocomposite coatings with enhanced corrosion inhibition effects for copper. *Int. J. Biol. Macromol.* **2020**, *162*, 1566–1577. [[CrossRef](#)]
38. Singh, A.; Ansari, K.R.; Quraishi, M.A. Inhibition effect of natural polysaccharide composite on hydrogen evolution and P110 steel corrosion in 3.5 wt% NaCl solution saturated with CO₂: Combination of experimental and surface analysis. *Int. J. Hydrog. Energy* **2020**, *45*, 25398–25408. [[CrossRef](#)]
39. Kumar, K.V.; Appa Rao, V.B. Phosphorylated xanthan gum, an environment-friendly, efficient inhibitor for mild steel corrosion in aqueous 200 ppm NaCl. *Mater. Today Proc.* **2019**, *15*, 155–165. [[CrossRef](#)]
40. Bertalan, G.; Ruzsna, I.; Anna, P.; Boros-Ivics, M.; Marosi, G. Mechanism and kinetics of hydrochloric acid initiated ε-caprolactam polymerization: 1. The role of stereoelectronic control and acid catalysis. *Polym. Bull.* **1988**, *19*, 539–546. [[CrossRef](#)]
41. Singh, A.; Ansari, K.R.; Ituen, E.; Guo, L.; Wahab, A.; Quraishi, M.; Kong, X.; Lin, Y. A new series of synthesized compounds as corrosion mitigator for storage tanks: Detailed electrochemical and theoretical investigations. *Constr. Build. Mater.* **2020**, *259*, 120421. [[CrossRef](#)]

42. Daoud, D.; Douadi, T.; Hamani, H.; Chafaa, S.; Al-Noaimi, M. Corrosion inhibition of mild steel by two new S-heterocyclic compounds in 1 M HCl: Experimental and computational study. *Corros. Sci.* **2015**, *94*, 21–37. [[CrossRef](#)]
43. Muthukrishnan, P.; Jeyaprabha, B.; Prakash, P. Adsorption and corrosion inhibiting behavior of Lanneacoromandelica leaf extract on mild steel corrosion. *Arab. J. Chem.* **2017**, *10*, 2343–2354. [[CrossRef](#)]
44. Solomon, M.M.; Gerengi, H.; Umoren, S.A. Carboxymethyl Cellulose/Silver Nanoparticles Composite: Synthesis, Characterization and Application as a Benign Corrosion Inhibitor for St37 Steel in 15% H₂SO₄ Medium. *ACS Appl. Mater. Interfaces* **2017**, *9*, 6376–6379. [[CrossRef](#)]
45. Khalil, N. Quantum chemical approach of corrosion inhibition. *Electrochimica Acta* **2003**, *48*, 2635–2640. [[CrossRef](#)]
46. Zhang, F.; Tang, Y.; Cao, Z. Performance and theoretical study on corrosion inhibition of 2-(4-pyridyl)-benzimidazole for mild steel in hydrochloric acid. *Corros. Sci.* **2012**, *61*, 1–9. [[CrossRef](#)]
47. Ituen, E.; Akaranta, O.; James, A.; Sun, S. Green and sustainable local biomaterials for oilfield chemicals *Griffonia simplicifolia* extract as steel corrosion inhibitor in hydrochloric acid. *Sustain. Mater. Technol.* **2017**, *11*, 12–18. [[CrossRef](#)]
48. Salarvand, Z.; Amirnasr, M.; Talebian, M.; Raeissi, K.; Meghdadi, M. Enhanced corrosion resistance of mild steel in 1 M HCl solution by trace amount of 2-phenyl-benzothiazole derivatives: Experimental, quantum chemical calculations and molecular dynamics (MD) simulation studies. *Corros. Sci.* **2017**, *114*, 133–145. [[CrossRef](#)]